

The GAPS programme with HARPS-N@TNG IV: A planetary system around XO-2S *

S. Desidera¹, A.S. Bonomo², R.U. Claudi¹, M. Damasso^{2,3}, K. Biazzo⁴, A. Sozzetti², F. Marzari^{5,1}, S. Benatti¹, D. Gandolfi^{4,6}, R. Gratton¹, A.F. Lanza⁴, V. Nascimbeni^{7,1}, G. Andreuzzi⁸, L. Affer⁹, M. Barbieri⁷, L.R. Bedin¹, A. Bignamini¹⁰, M. Bonavita¹, F. Borsa¹¹, P. Calcidese³, J.M. Christille^{3,12}, R. Cosentino^{4,8}, E. Covino¹³, M. Esposito¹⁴, P. Giacobbe², A. Harutyunyan⁸, D. Latham¹⁵, M. Lattanzi², G. Leto⁴, G. Lodato¹⁶, C. Lovis¹⁷, A. Maggio⁹, L. Malavolta^{7,17}, L. Mancini¹⁸, A.F. Martinez Fiorenzano⁸, G. Micela⁹, E. Molinari^{8,19}, C. Mordasini¹⁸, U. Munari¹, I. Pagano⁴, M. Pedani⁸, F. Pepe¹⁷, G. Piotto^{7,1}, E. Poretti¹¹, M. Rainer¹¹, I. Ribas²⁰, N.C. Santos^{21,22}, G. Scandariato⁴, R. Silvotti², J. Southworth²³, R. Zanmar Sanchez⁴

- ¹ INAF – Osservatorio Astronomico di Padova, Vicolo dell'Osservatorio 5, I-35122, Padova, Italy
- ² INAF – Osservatorio Astrofisico di Torino, Via Osservatorio 20, I-10025, Pino Torinese, Italy
- ³ Osservatorio Astronomico della Regione Autonoma Valle d'Aosta, Fraz. Lignan 39, I-11020, Nus (Aosta), Italy
- ⁴ INAF – Osservatorio Astrofisico di Catania, Via S.Sofia 78, I-95123, Catania, Italy
- ⁵ Dipartimento di Fisica e Astronomia Galileo Galilei – Università di Padova, Via Marzolo 8, I-35131 Padova, Italy
- ⁶ Landessternwarte Königstuhl, ZAH, Universität Heidelberg, Königstuhl 12, D-69117 Heidelberg, Germany
- ⁷ Dip. di Fisica e Astronomia Galileo Galilei – Università di Padova, Vicolo dell'Osservatorio 2, I-35122, Padova, Italy
- ⁸ Fundación Galileo Galilei - INAF, Rambla José Ana Fernández Pérez 7, E-38712 Breña Baja, TF - Spain
- ⁹ INAF – Osservatorio Astronomico di Palermo, Piazza del Parlamento, Italy 1, I-90134, Palermo, Italy
- ¹⁰ INAF – Osservatorio Astronomico di Trieste, via Tiepolo 11, I-34143 Trieste, Italy
- ¹¹ INAF – Osservatorio Astronomico di Brera, Via E. Bianchi 46, I-23807 Merate (LC), Italy
- ¹² Dept. of Physics, University of Perugia, via A. Pascoli 1, 06123, Perugia, Italy
- ¹³ INAF – Osservatorio Astronomico di Capodimonte, Salita Moiariello 16, I-80131, Napoli, Italy
- ¹⁴ Instituto de Astrofísica de Canarias, C/Vía Lactea S/N, E-38200 La Laguna, Tenerife, Spain
- ¹⁵ Harvard-Smithsonian Center for Astrophysics, 60 Garden Street, Cambridge, MA 02138
- ¹⁶ Dipartimento di Fisica, Università di Milano, Via Celoria 16, I-20133 Milano, Italy
- ¹⁷ Obs. Astronomique de l'Univ. de Geneve, 51 ch. des Maillettes - Sauvigny, CH-1290, Versoix, Switzerland
- ¹⁸ Max-Planck-Institut für Astronomie, Königstuhl 17, D-69117, Heidelberg, Germany
- ¹⁹ INAF - IASF Milano, via Bassini 15, I-20133 Milano, Italy
- ²⁰ Inst. de Ciències de l'Espai (CSIC-IEEC), Campus UAB, Facultat de Ciències, 08193 Bellaterra, Spain
- ²¹ Centro de Astrofísica, Universidade do Porto, Rua das Estrelas, 4150-762 Porto, Portugal
- ²² Departamento de Física e Astronomia, Faculdade de Ciências, Universidade do Porto, Portugal
- ²³ Astrophysics Group, Keele University, Staffordshire, ST5 5BG, UK

ABSTRACT

We performed an intensive radial velocity monitoring of XO-2S, the wide companion of the transiting planet-host XO-2N, using HARPS-N at TNG in the framework of the GAPS programme. The radial velocity measurements indicate the presence of a new planetary system formed by a planet that is slightly more massive than Jupiter at 0.48 au and a Saturn-mass planet at 0.13 au. Both planetary orbits are moderately eccentric and were found to be dynamically stable. There are also indications of a long-term trend in the radial velocities. This is the first confirmed case of a wide binary whose components both host planets, one of which is transiting, which makes the XO-2 system a unique laboratory for understanding the diversity of planetary systems.

Key words. (Stars:) individual: XO-2S, XO-2N — planetary systems — techniques: radial velocities

1. Introduction

The discoveries of extrasolar planets in the past two decades have revealed a surprising variety of system architectures

and planet characteristics. The wide diversity of the outcomes of the planet formation process is linked to the properties of the host stars, the characteristics of the circumstellar disks, and the effects of the environment in which the stars and their planets form and evolve (Mordasini et al. 2012).

* Based on observations made with the Italian Telescopio Nazionale Galileo (TNG) operated on the island of La Palma by the Fundación Galileo Galilei of the INAF at the Spanish Observatorio del Roque de los Muchachos of the IAC in the frame of the program Global Architecture of Planetary Systems (GAPS), and on observations made at Asiago, Serra La Nave, and Valle D'Aosta Observatories.

A better understanding of the stochastic factors that affect planet formation can be achieved by observing wide binary systems with similar components. This allows some of the relevant variables (chemical composition, birth environment, age) to be the same for both components. On the

other hand, the presence of stellar companions can affect the dynamical evolution of planetary systems. Kaib et al. (2013) showed that even very wide binaries ($a \sim 1000$ au) can have a significant impact on the survival and orbital properties of any planets they might host, because of the continuous evolution of the binaries' orbital elements caused by interactions with passing stars and Galactic tides. Indeed, some differences in the properties of planets in binaries with respect to those orbiting single stars have been identified, such as the excess of massive close-in planets (Desidera & Barbieri 2007) and of planets on highly eccentric orbits (Kaib et al. 2013).

With a few exceptions (Desidera et al. 2011; Toyota et al. 2009), radial velocity (RV) surveys have historically excluded known binaries from their samples, or included only one component of optically resolved systems, depending on the adopted selection criteria. Furthermore, the probability to have planets transiting each component of a binary system is low, and resolving the binary is challenging for stars at the typical distance of the targets of transit surveys. Nevertheless, some candidates have been identified by the *Kepler* mission, with Kepler-132 being the most promising one (Lissauer et al. 2014). However, the available data only allow the conclusion that the planet candidates orbit different components. The identification of the host of each transiting object remains ambiguous, and further characterization is hampered by the faintness of the stars and their small angular separation.

Another possibility is to search for planets around the companions of known planet hosts. Stars with planets are often the subject of searches for stellar companions (e.g., Chauvin et al. 2006; Mugrauer et al. 2014), or common proper motion stars may be known well before the discovery of planets (Raghavan et al. 2006). In this letter we present the results of intensive RV monitoring of the K0 star XO-2S (TYC 3413-210-1), performed using the spectrograph HARPS-N (Cosentino et al. 2012) at the Telescopio Nazionale Galileo (TNG) as part of the programme Global Architecture of Planetary Systems (GAPS, Covino et al. 2013; Desidera et al. 2013). XO-2S ($V=11.12$ mag; $B - V=0.79$) is the wide ($30''$, ~ 4000 au projected separation) companion of XO-2N, which was found to host a transiting planet of mass $0.5 M_J$ and orbital period 2.5 d (Burke et al. 2007). The two components are very similar ($\Delta R \sim 0.04$ mag), and both are super-metal-rich in composition. Our observations allowed us to detect two giant planets around XO-2S, both at orbital separations larger than the hot Jupiter around XO-2N, thus making the XO-2 system the first confirmed case of a wide binary whose components both host planets, one of which is transiting. Here we report the RV measurements, stellar activity and line profile indicators, ancillary photometric observations taken at the Asiago, Valle d'Aosta and Serra La Nave Observatories supporting the Keplerian origin of the RV variations, the planet parameters, and the evaluation of the dynamical stability of the system. In a forthcoming paper (Damasso et al., in prep.) we will present a complete analysis of the XO-2 system.

2. Observations and data reduction

The system XO-2S was observed with HARPS-N at 63 individual epochs between April 2013 and May 2014. The Th-Ar simultaneous calibration was not used to avoid

Table 1. XO-2S stellar parameters

Parameter	Value
T_{eff} (K)	5399 ± 55
$\log g$ (cgs)	4.43 ± 0.08
[Fe/H] (dex)	0.39 ± 0.05
Microturb. (km s^{-1})	0.9 ± 0.1
Mass (M_{\odot})	0.982 ± 0.054
Radius (R_{\odot})	$1.02^{+0.09}_{-0.07}$
Age (Gyr)	$7.1^{+2.5}_{-2.9}$
$v \sin i$ (km s^{-1})	1.7 ± 0.4
$\log R_{HK}$	-5.03

contamination of the stellar spectrum by the lamp lines (which might affect a proper spectral analysis; Sect. 3). Nevertheless, the drift correction with respect to the reference calibration shows a dispersion of just 0.8 m s^{-1} , which is of very limited impact considering the typical photon-noise RV error of 2.2 m s^{-1} .

The reduction of the spectra and the RV measurements were obtained using the latest version (Nov. 2013) of the HARPS-N instrument data reduction software pipeline and the K5 mask. The measurement of the RVs is based on the weighted cross-correlation function (CCF) method (Baranne et al. 1996; Pepe et al. 2002).

3. Stellar parameters

The extracted spectra of XO-2S were coadded to produce a merged spectrum with a peak S/N ratio of about 200 at 550 nm. We determined the stellar parameters using implementations of both the equivalent width and the spectral synthesis methods, as described in Esposito et al. (2014) and Santos et al. (2013). We also used the infrared flux method to estimate T_{eff} . The results agree very well with each other. The adopted parameters are the weighted averages of the individual results (Table 1). Full details will be given in Damasso et al. (in prep.).

The stellar mass, radius, and age were estimated using the Yonsei-Yale evolutionary tracks (Demarque et al. 2004) that match the effective temperature, iron abundance, and surface gravity of XO-2S (Table 1). The adopted errors include an additional 5% in mass and 3% in radius added in quadrature to the formal errors to take systematic uncertainties in stellar models into account (Southworth 2011).

The star was found to be a slow rotator (using a preliminary calibration of the FWHM of the CCF and spectral synthesis) that exhibits low levels of chromospheric emission. Other age diagnostics (kinematics, lack of detectable amounts of lithium) support the old age of the system and confirm the findings by Burke et al. (2007).

4. RV variations and their origin

The relative RV time series is shown in Fig. 1. We report in Table 2 the full dataset. The RVs show a dispersion of 34.3 m s^{-1} , significantly exceeding the measurement errors. A Lomb-Scargle periodogram yields the most significant power at a period of 120 d. The RV semi-amplitude resulting from a Keplerian fit is $K = 58 \text{ m s}^{-1}$. Moreover, the post-fit residuals show additional modulations with a

period of 18.3 d¹. A test based on bootstrap random permutation shows that this periodicity is highly significant, with a false-alarm probability lower than 10⁻⁴, and a corresponding semi-amplitude $K \sim 20 \text{ m s}^{-1}$. The period value, however, is fairly typical of rotational periods of old, solar-type dwarfs. Therefore, we performed specific checks to exclude rotational modulations and other stellar phenomena as the origin of the RV variations.

We first searched for correlations between the RVs and line profile indicators, considering the bisector velocity span as delivered by the HARPS-N pipeline and our own implementation of the diagnostics proposed by Figueira et al. (2013). We also derived indices to measure the chromospheric activity in the CaII H&K and H α lines. None of these indices show either significant power at the RV periods or significant correlations with the original RVs or the residuals of the one-planet fit (Fig. 3).

To further exclude stellar variability as the origin of the observed RV signals, we obtained accurate multi-band photometry at the Asiago, Serra La Nave and Aosta Valley observatories. The latter was used to monitor XO-2S during 42 nights from 2 Dec 2013 to 8 Apr 2014 in the *I* band, following the observations and data reduction procedure of the APACHE program (Sozzetti et al. 2013; Christille et al. 2013). At Serra La Nave we observed in *B*, *V*, *R*, *I* bands on four nights in 2013-2014. We also analyzed data of the XO-2 system acquired at Asiago in the context of the TASTE program (Nascimbeni et al. 2011) during ten nights in which transits of the hot-Jupiter in front of XO-2N occurred. The APACHE time series shows a scatter of 0.003 mag (nightly averages), without significant power at the period of the RV variations. The nightly averages of the Asiago and Serra La Nave datasets show a similar scatter in the magnitude difference between XO-2N and XO-2S, confirming the low level of photometric variability of the two stars. The photometric amplitude due to star-spots associated with an activity-induced RV variation with a semi-amplitude of 20 m s⁻¹ (derived using Eq. 1 of Desort et al. 2007) is about 3%, which is one order of magnitude larger than the observed photometric variability.

In summary, the tests performed allowed us to rule out phenomena related to stellar activity and rotation as the cause of the observed RV variations with periods of ~ 120 and ~ 18 d. We conclude that these are due to Keplerian motions, which are characterized in Sect. 5.

5. Orbital parameters and dynamical stability

Orbital parameters and associated uncertainties were determined with a Bayesian differential evolution Markov chain Monte Carlo analysis of the HARPS-N data (Ter Braak 2006; Eastman et al. 2013) by maximizing a Gaussian likelihood function (e.g., Ford 2006). Our two-planet model has 13 free parameters: periastron epoch T_0 , orbital period P , K , $\sqrt{e} \cos \omega$, and $\sqrt{e} \sin \omega$ of the two planets XO-2Sb and c, e and ω being the eccentricity and the argument of periastron, the systemic velocity γ , a slope, and a jitter term (e.g., Gregory 2005), which includes RV scatter that is possibly induced by stellar variability and/or

¹ During eight observing nights, the spectra were obtained twice per night with a separation of a few hours to investigate the possibility of aliases. These data corroborated the 18.3 d periodicity.

Table 3. Orbital parameters

Parameter	XO-2Sb	XO-2Sc
P (d)	18.157 ± 0.034	120.80 ± 0.34
K (m s ⁻¹)	20.64 ± 0.85	57.68 ± 0.69
$\sqrt{e} \sin \omega$	$-0.314^{+0.059}_{-0.052}$	$-0.388^{+0.013}_{-0.012}$
$\sqrt{e} \cos \omega$	$0.282^{+0.054}_{-0.065}$	$-0.038^{+0.033}_{-0.034}$
e	0.180 ± 0.035	$0.1528^{+0.0094}_{-0.0098}$
ω (deg)	311.9 ± 9.5	264.5 ± 4.9
T_0 (BJD _{TDB} -2450000)	$6413.11^{+0.82}_{-0.86}$	$6408.1^{+1.8}_{-1.9}$
T_c (BJD _{TDB} - 2450000)	6419.30 ± 0.53	$6471.02^{+0.85}_{-0.90}$
slope (m s ⁻¹ d ⁻¹)	0.0531 ± 0.0087	
γ (km s ⁻¹)	46.543 ± 0.001	
jitter (m s ⁻¹)	1.80 ± 0.43	
rms (m s ⁻¹)	3.1	
$m \sin i$ (M _{Jup})	0.259 ± 0.014	1.370 ± 0.053
a (AU)	0.1344 ± 0.0025	0.4756 ± 0.0087

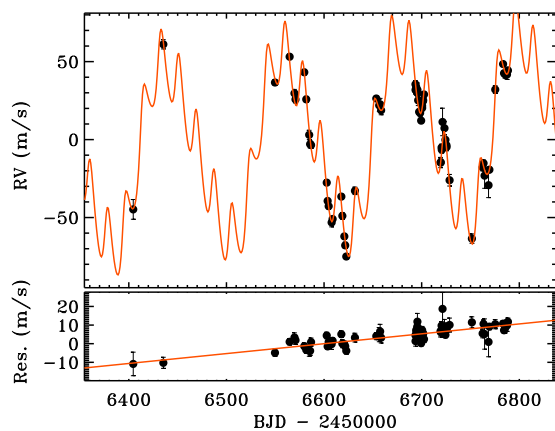


Fig. 1. Upper panel: relative RVs of XO-2S. The overplotted line is the best-fit Keplerian solution for two planets and a linear trend. Lower panel: residuals of XO-2S RVs after removing the contribution of the two planets XO-2Sb and XO-2Sc. The overplotted line is the best-fit linear trend.

instrumental noise that exceeds the nominal error bars. Uninformative priors were used for all parameters. Twenty-six chains were run simultaneously, and were stopped after convergence and good mixing of the chains were reached according to Ford (2006). Burn-in steps were removed following Eastman et al. (2013). The medians of the parameter posterior distributions and their 34.13% intervals are taken as final values and their 1- σ uncertainties, respectively. The results are listed in Table 3 and shown in Fig. 2.

The two planets have moderately eccentric orbits: $e = 0.180 \pm 0.035$ (XO-2Sb) and 0.153 ± 0.010 (XO-2Sc). The inferred minimum masses are 0.259 ± 0.014 and $1.370 \pm 0.053 M_{\text{Jup}}$ for planets b and c, respectively. Interestingly, we found evidence at the 6- σ level for a long-term trend of $0.053 \pm 0.009 \text{ m s}^{-1} \text{ d}^{-1}$ (Fig. 1) in the residuals of the two-planet fit. This is likely due to an additional companion whose nature remains to be established. The trend cannot be due to the wide companion XO-2N because of its very large separation (a slope of the order of $10^{-5} \text{ m s}^{-1} \text{ d}^{-1}$ is expected). The orbital parameters of the two planetary companions are only marginally affected by the inclusion of the long-term RV slope.

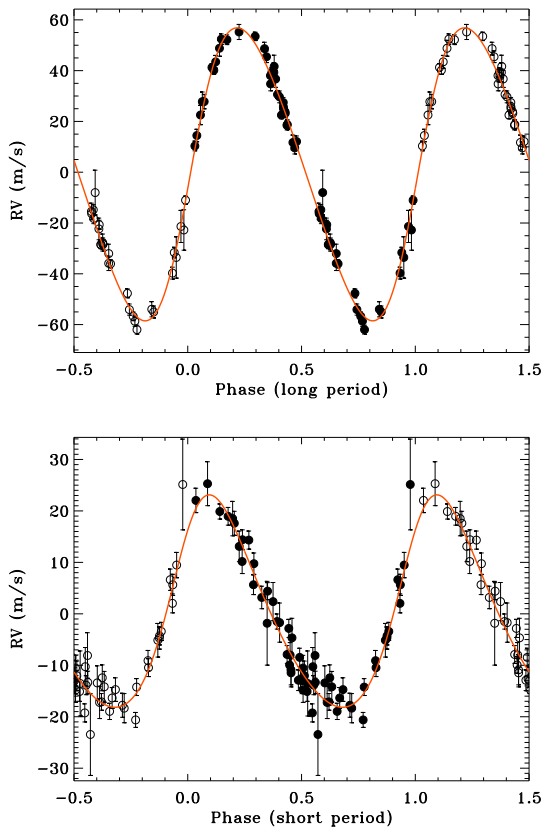


Fig. 2. Phased plot for the two planets orbiting XO-2S. In each panel, the RV signal of the other object and the long-term trend are subtracted. Upper panel: long-period planet (XO-2Sc). Lower panel: short-period planet (XO-2Sb).

Finally, we performed a dynamical analysis of the proposed best fit of the planetary system. We have numerically integrated the nominal system (assuming nearly coplanar orbits) over 100 Myr using the symplectic integrator SyMBA (Duncan et al. 1998) and found a stable quasi-periodic evolution. We also used the frequency map analysis, as described in Marzari et al. (2005), to explore the stability properties close to the nominal solution. We found very low diffusion values when sampling the initial conditions in a random way within the error bars of all orbital elements and of the estimated planetary and stellar masses. This indicates that the system is located in a robustly stable area of the phase space.

6. Discussion and conclusions

Based on high-precision HARPS-N Doppler measurements, we presented the discovery of a planetary system composed of a planet slightly more massive than Jupiter at 0.48 au and a Saturn-mass planet at 0.13 au around XO-2S, the wide companion of the transiting hot-Jupiter host XO-2N. The two planetary orbits are moderately eccentric and were found to be dynamically stable. There are also indications of a long-term trend in the RVs. A longer time baseline of the observations is needed to infer its origin. The two planets have periods intermediate between the hot-Jupiter pile-up and the rise in frequency at $a \geq 1$ au, which means that they are located in the so-called period-valley in the

distribution of known exoplanets (Wittenmyer et al. 2010). The geometric transit probabilities for the inner and outer planets are 3% and 1%, respectively. However, the available photometric data and the uncertainties on the transit epochs (Table 3) do not allow us to set any meaningful constraints on the occurrence of their transits.

This is the first confirmed case of a wide binary whose components both host planets, one of which is transiting. The two stars are almost twins but the planetary systems around them are not, with one component hosting a hot-Jupiter and the other one hosting a Jupiter and a Saturn-mass planet in wider orbits. This fact makes this system a special laboratory for our understanding of planet formation processes and the influence of specific classes of planets on their parent stars, for example in terms of alteration of the chemical composition (Ramírez et al. 2010) and angular momentum (Lanza 2010; Poppenhaeger & Wolk 2014). We plan to address these questions in forthcoming publications.

Acknowledgements. The GAPS project in Italy acknowledges support from INAF through the “Progetti Premiali” funding scheme of the Italian Ministry of Education, University, and Research. The Aosta Valley Observatory is supported by the Regional Government of the Aosta Valley, the Town Municipality of Nus and the Mont Emilius Community. JMC is supported by a grant of the EU-ESF, the Autonomous Region of the Aosta Valley and the Italian Ministry of Labour and Social Policy. We thank ASI (through contracts I/037/08/0 and I/058/10/0) and the Fondazione CRT for their support to the APACHE Project. DG acknowledges support from the EU FP7 under grant agreement n. 267251. NCS acknowledges support from Fundação para a Ciência e a Tecnologia (FCT, Portugal) through the FEDER funds in the program COMPETE, as well as through national funds, in the form of grants reference RECI/FIS-AST/0176/2012 (FCOMP-01-0124-FEDER-027493), and RECI/FIS-AST/0163/2012 (FCOMP-01-0124-FEDER-027492), and in the form of the Investigador FCT contract reference IF/00169/2012 and POPH/FSE (EC) by the FEDER funding through the program “Programa Operacional de Factores de Competitividade - COMPETE. NCS furthermore acknowledges the support from the ERC/EC under the FP7 through Starting Grant agreement n. 239953. We thank the TNG staff for help with the observations.

References

- Baranne, A., Queloz, D., Mayor, M., et al. 1996, *A&AS*, 119, 373
- Burke, C. J., McCullough, P. R., Valenti, J. A., et al. 2007, *ApJ*, 671, 2115
- Chauvin, G., Lagrange, A.-M., Udry, S., et al. 2006, *A&A*, 456, 1165
- Christille, J.-M., Bernagozzi, A., Bertolini, E., et al. 2013, in *European Physical Journal Web of Conferences*, Vol. 47, European Physical Journal Web of Conferences, 17001
- Cosentino, R., Lovis, C., Pepe, F., et al. 2012, in *Society of Photo-Optical Instrumentation Engineers (SPIE) Conference Series*, Vol. 8446, Society of Photo-Optical Instrumentation Engineers (SPIE) Conference Series
- Covino, E., Esposito, M., Barbieri, M., et al. 2013, *A&A*, 554, A28
- Demarque, P., Woo, J.-H., Kim, Y.-C., & Yi, S. K. 2004, *ApJS*, 155, 667
- Desidera, S. & Barbieri, M. 2007, *A&A*, 462, 345
- Desidera, S., Carolo, E., Gratton, R., et al. 2011, *A&A*, 533, A90
- Desidera, S., Sozzetti, A., Bonomo, A. S., et al. 2013, *A&A*, 554, A29
- Desort, M., Lagrange, A.-M., Galland, F., Udry, S., & Mayor, M. 2007, *A&A*, 473, 983
- Duncan, M. J., Levison, H. F., & Lee, M. H. 1998, *AJ*, 116, 2067
- Eastman, J., Gaudi, B. S., & Agol, E. 2013, *PASP*, 125, 83
- Esposito, M., Covino, E., Mancini, L., et al. 2014, *A&A*, 564, L13
- Figuera, P., Santos, N. C., Pepe, F., Lovis, C., & Nardetto, N. 2013, *A&A*, 557, A93
- Ford, E. B. 2006, *ApJ*, 642, 505
- Gregory, P. C. 2005, *ApJ*, 631, 1198
- Kaib, N. A., Raymond, S. N., & Duncan, M. 2013, *Nature*, 493, 381
- Lanza, A. F. 2010, *A&A*, 512, A77

- Lissauer, J. J., Marcy, G. W., Bryson, S. T., et al. 2014, *ApJ*, 784, 44
- Marzari, F., Scholl, H., & Tricarico, P. 2005, *A&A*, 442, 359
- Mordasini, C., Alibert, Y., Benz, W., Klahr, H., & Henning, T. 2012, *A&A*, 541, A97
- Mugrauer, M., Ginski, C., & Seeliger, M. 2014, *MNRAS*, 439, 1063
- Nascimbeni, V., Piotto, G., Bedin, L. R., & Damasso, M. 2011, *A&A*, 527, A85
- Pepe, F., Mayor, M., Galland, F., et al. 2002, *A&A*, 388, 632
- Poppenhaeger, K. & Wolk, S. J. 2014, *A&A*, 565, L1
- Raghavan, D., Henry, T. J., Mason, B. D., et al. 2006, *ApJ*, 646, 523
- Ramírez, I., Asplund, M., Baumann, P., Meléndez, J., & Bensby, T. 2010, *A&A*, 521, A33
- Santos, N. C., Sousa, S. G., Mortier, A., et al. 2013, *A&A*, 556, A150
- Southworth, J. 2011, *MNRAS*, 417, 2166
- Sozzetti, A., Bernagozzi, A., Bertolini, E., et al. 2013, in *European Physical Journal Web of Conferences*, Vol. 47, *European Physical Journal Web of Conferences*, 3006
- Ter Braak, C. J. F. 2006, *Statistics and Computing*, 16, 239
- Toyota, E., Itoh, Y., Ishiguma, S., et al. 2009, *PASJ*, 61, 19
- Wittenmyer, R. A., O'Toole, S. J., Jones, H. R. A., et al. 2010, *ApJ*, 722, 1854

Table 2. Radial velocities, bisector velocity span, and $\log R_{HK}$ of XO-2S. The errors on the bisector velocity span are about twice as high as the errors on radial velocities.

BJD _{UTC} - 2 450 000	RV (km s ⁻¹)	error (km s ⁻¹)	Bisector (km s ⁻¹)	$\log R_{HK}$	err $\log R_{HK}$
6404.52027	46.4982	0.0063	0.0069	-5.478	0.584
6435.37047	46.6041	0.0030	0.0111	-5.263	0.111
6549.73055	46.5796	0.0019	0.0034	-5.126	0.045
6564.73154	46.5961	0.0017	0.0078	-5.020	0.028
6569.69948	46.5727	0.0025	0.0078	-5.054	0.057
6570.74915	46.5688	0.0023	0.0051	-5.134	0.059
6579.73878	46.5862	0.0017	0.0097	-5.109	0.035
6581.76437	46.5688	0.0019	0.0107	-5.006	0.034
6584.75753	46.5460	0.0029	0.0039	-5.070	0.071
6585.72086	46.5401	0.0024	-0.0031	-5.083	0.055
6586.70194	46.5395	0.0022	0.0002	-5.000	0.040
6602.73935	46.5154	0.0018	0.0061	-5.053	0.033
6603.67615	46.5036	0.0016	0.0123	-4.993	0.025
6604.72411	46.5003	0.0019	0.0075	-5.053	0.035
6607.76170	46.4898	0.0028	0.0172	-5.100	0.075
6608.75358	46.4921	0.0016	0.0040	-5.061	0.030
6617.70822	46.5064	0.0018	0.0050	-4.981	0.027
6618.73859	46.4941	0.0022	0.0118	-5.053	0.045
6620.76267	46.4809	0.0017	0.0085	-5.053	0.032
6621.65931	46.4751	0.0020	0.0055	-5.090	0.045
6622.77386	46.4680	0.0018	0.0061	-4.996	0.029
6631.64148	46.5101	0.0024	0.0071	-5.008	0.048
6653.51105	46.5693	0.0019	0.0055	-5.100	0.043
6656.47923	46.5649	0.0038	0.0074	-5.004	0.091
6657.46522	46.5656	0.0038	0.0014	-5.198	0.143
6658.45326	46.5618	0.0029	0.0104	-5.077	0.075
6693.63057	46.5785	0.0024	0.0036	-5.006	0.049
6693.70485	46.5749	0.0027	0.0060	-4.913	0.050
6694.39223	46.5767	0.0018	0.0095	-4.976	0.028
6694.65433	46.5742	0.0025	0.0103	-5.000	0.048
6695.44269	46.5730	0.0037	0.0117	-4.901	0.064
6695.62098	46.5749	0.0044	0.0085	-5.106	0.131
6696.39858	46.5681	0.0033	0.0027	-4.963	0.064
6697.38288	46.5608	0.0016	0.0021	-5.026	0.026
6698.40230	46.5600	0.0023	0.0011	-4.995	0.042
6699.45786	46.5551	0.0014	0.0046	-5.038	0.023
6700.44799	46.5647	0.0020	0.0085	-4.987	0.034
6700.48597	46.5633	0.0017	0.0136	-5.027	0.030
6701.36430	46.5677	0.0018	0.0043	-5.009	0.032
6701.50593	46.5683	0.0018	0.0014	-5.033	0.031
6702.39608	46.5719	0.0019	0.0005	-5.051	0.035
6719.38765	46.5283	0.0033	0.0119	-5.039	0.099
6719.51119	46.5284	0.0021	0.0006	-4.999	0.039
6720.38049	46.5379	0.0021	0.0040	-5.007	0.038
6720.58213	46.5365	0.0021	0.0038	-5.064	0.043
6721.37526	46.5543	0.0088	0.0067	-5.030	0.254
6723.35649	46.5503	0.0043	0.0035	-5.008	0.104
6724.33597	46.5429	0.0015	-0.0024	-4.984	0.021
6725.35840	46.5394	0.0034	0.0169	-5.137	0.101
6725.49169	46.5382	0.0023	0.0028	-5.028	0.047
6728.58121	46.5169	0.0037	0.0116	-4.985	0.085
6751.42778	46.4795	0.0030	0.0046	-5.008	0.068
6762.42972	46.5252	0.0023	-0.0014	-5.053	0.056
6763.36878	46.5278	0.0021	0.0069	-4.962	0.037
6764.42477	46.5199	0.0081	0.0130	-4.899	0.192
6768.47748	46.5137	0.0080	0.0277	-4.836	0.197
6769.36163	46.5237	0.0016	0.0067	-5.061	0.032
6775.36013	46.5751	0.0025	0.0072	-5.150	0.075
6783.37304	46.5915	0.0015	0.0039	-5.033	0.026
6784.37312	46.5856	0.0016	0.0026	-5.039	0.031
6785.36182	46.5849	0.0025	0.0037	-5.178	0.082
6787.36842	46.5847	0.0031	-0.0020	-5.126	0.102
6788.37059	46.5873	0.0020	0.0041	-5.009	0.042

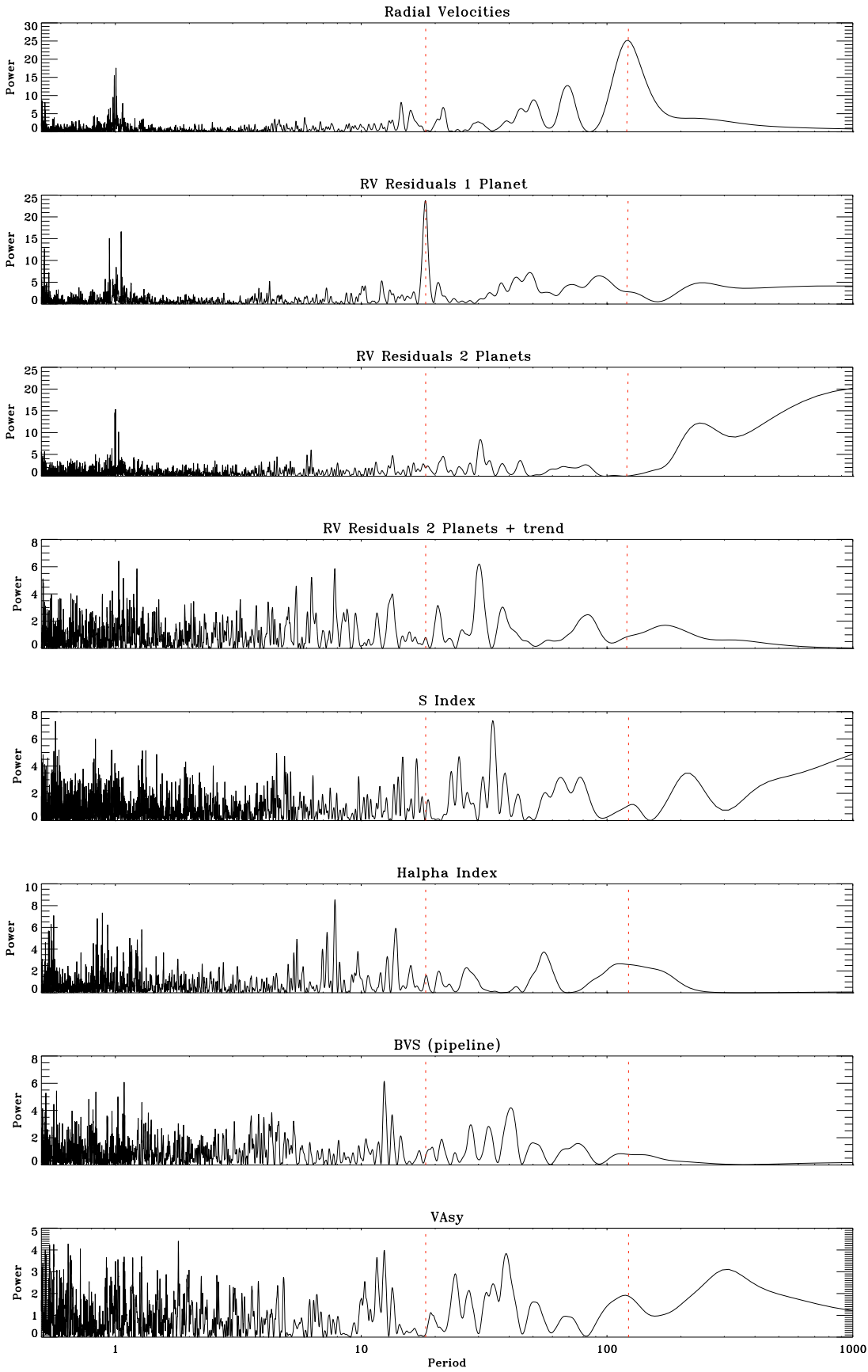


Fig. 3. Lomb-Scargle periodogram of RV and activity indicators of XO-2S. From top to bottom: raw RVs, one-planet fit residuals, two-planet fit residuals, two-planet plus linear-trend fit residuals; H and K S index, $H\alpha$ index, bisector velocity span, V_{asy} indicator (see [Figueira et al. 2013](#)). In all panels the periodicities of the two planetary companions are marked with vertical dashed lines.